Covalency-Driven Preservation of Local Charge Densities in a Metal-to-Ligand Charge-Transfer Excited Iron Photosensitizer

Raphael M. Jay,* Sebastian Eckert, Vinícius Vaz da Cruz, Mattis Fondell, Rolf Mitzner, and Alexander Föhlisch*

Abstract: *Covalency is found to even out charge separation after photo-oxidation of the metal center in the metal-to-ligand charge-transfer state of an iron photosensitizer. The σ-donation ability of the ligands compensates for the loss of iron 3d electronic charge, thereby upholding the initial metal charge density and preserving the local noble-gas configuration. These findings are enabled through element-specific and orbital-selective time-resolved X-ray absorption spectroscopy at the iron L-edge. Thus, valence orbital populations around the central metal are directly accessible. In conjunction with density functional theory we conclude that the picture of a localized charge-separation is inadequate. However, the unpaired spin density provides a suitable representation of the electron–hole pair associated with the electron-transfer process.*

Creating electron–hole pairs via the absorption of visible light is the basic principle underlying all photo-voltaic applications. In dye-sensitized solar cells, charge carriers are often generated by transition-metal complexes, where the absorption of visible light populates metal-to-ligand charge-transfer (MLCT) states. As a result of their superior MLCT lifetimes, Ru^{II} complexes have been implemented in the most prominent realization, the Grätzel cell.[1] For widespread commercial application however, complexes based on more abundant metals are needed. Tremendous efforts are thus being directed towards improving the photochemical properties of Fe^{II} complexes whose low-lying metal-centered (MC)

states usually facilitate femtosecond relaxation of the initially populated MLCT states.[2–5] Employing strong σ-donating ligands to sufficiently destabilize MC states has proven a successful approach to inhibit ultrafast relaxation channels and push Fe^{II} MLCT lifetimes into the picosecond domain.[6–8]

While the excited-state potential energy landscape of Fe^{II} complexes can now be routinely tailored, we still lack a fundamental understanding of the valence electronic structure of charge-transfer states as the starting point of interfacial charge injection. They are commonly described by a locally oxidized/reduced metal site,[9–11] but the quantitative implications on charge and spin distributions are rather elusive. This is in particular the case in the light of quantum chemical simulations suggesting that oxidizing the transition metal center, that is, reducing the 3d electron count, does not strongly influence its local electronic charge.[12,13] Reconciling these observations with the demonstrated interfacial charge injection from MLCT states of Fe-based dyes[14–16] is therefore not only important in terms of a fundamental chemical understanding but also for the further development of low-cost and high-efficiency light-harvesting applications.

Herein, we show that the formation of a MLCT state in a Fe^{II} complex is only accompanied by a minor separation of electronic charge, as the depopulation of metal-centered orbitals can be efficiently compensated for by the strong metal-ligand covalency. We establish this general mechanism by studying the valence electronic structure of the ^{3}MLCT state of the complex $[Fe(bpy)(CN)_4]^{2-}$ using time-resolved X-ray absorption spectroscopy (XAS) at the Fe L-edge. The underlying 2p→3d excitation locally probes the density of unoccupied states around the metal center and is thereby sensitive to metal-ligand covalency,[17–19] the metal oxidation state[13,20] and local charge distribution.[21,22] Applied within an optical-pump X-ray-probe scheme, the method extends its sensitivity to valence-excited states by directly monitoring optically induced changes in the occupation of 3d-derived orbitals.[23] By combining time-resolved L-edge XAS with density functional theory (DFT) we can therefore provide a detailed analysis of the ^{3}MLCT valence electronic structure and relate the photo-induced spectral changes to variations in local charge and spin densities.

Figure 1a shows the nuclear geometry of $[Fe(bpy)-(CN)_4]^{2-}$ with its four cyanide (CN^-) and one 2-2′-bipyridine (bpy) ligand, thereby constituting a Fe^{II} closed-shell singlet within pseudo-octahedral symmetry. A strong solvatochromism is associated with the complex (see Figure 1b), that changes $Fe(t_{2g})→bpy(π^*)$ MLCT excitation energies as a function of the solvent environment. The high Lewis acidity of water withdraws electron density from the CN^- ligands

[*] R. M. Jay, Dr. S. Eckert, Dr. V. Vaz da Cruz, Prof. Dr. A. Föhlisch
Institut für Physik und Astronomie
Universität Potsdam
Karl-Liebknecht-Strasse 24/25, Potsdam (Germany)
E-mail: rajay@uni-potsdam.de

Dr. M. Fondell, Dr. R. Mitzner, Prof. Dr. A. Föhlisch
Institute for Methods and Instrumentation for Synchrotron Radiation Research, Helmholtz-Zentrum Berlin für Materialien und Energie GmbH
Albert-Einstein-Strasse 15, 12489 Berlin (Germany)
E-mail: alexander.foehlisch@helmholtz-berlin.de

Dr. S. Eckert
Current address: Max Born Institute for Nonlinear Optics and Short Pulse Spectroscopy
Max Born Strasse 2A, 12489 Berlin (Germany)

Supporting information and the ORCID identification number(s) for the author(s) of this article can be found under:
https://doi.org/10.1002/anie.201904761.

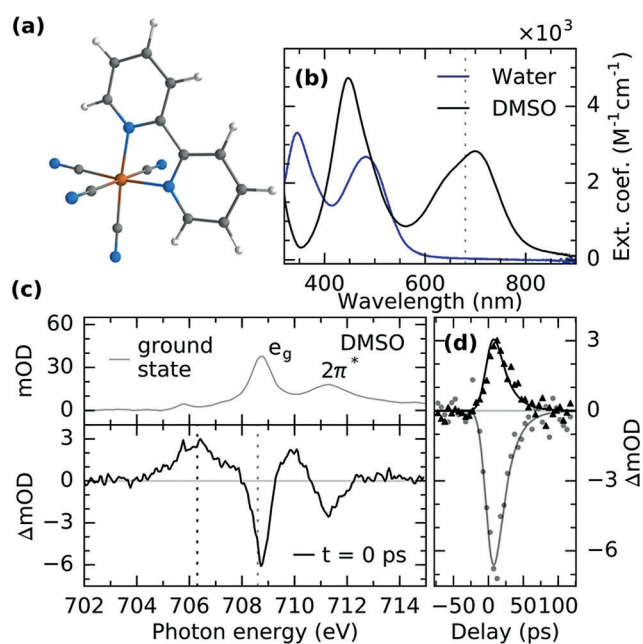**Figure 1.** a) Nuclear geometry and b) optical absorption spectra of [Fe(bpy)(CN)$_4$]$^{2-}$ in water and DMSO. c) Transient L$_3$-edge absorption spectrum of [Fe(bpy)(CN)$_4$]$^{2-}$ in DMSO compared to the ground state spectrum. d) Delay traces measured at the energies marked in the transient spectrum yielding a ^{3}MLCT lifetime of (17 ± 2) ps.

which is compensated for by a concomitant increase in π-back-donation. This has a stabilizing effect on the electronic ground state and therefore increases MLCT excitation energies.[24] Gaffney and co-workers determined the lowest MLCT state of [Fe(bpy)(CN)$_4$]$^{2-}$ in water to be energetically above metal-centered states.[25] Spin crossover from the initially photo-excited ^{1}MLCT to the ^{3}MLCT state therefore mediates femtosecond relaxation to a ^{3}MC state. In DMSO on the other hand, the stabilization of MLCT excitation energies results in the ^{3}MLCT state being the lowest valence-excited state exhibiting an extended lifetime of 19 ps.[8]

Figure 1c shows the transient L$_3$-edge absorption difference spectrum of [Fe(bpy)(CN)$_4$]$^{2-}$ in DMSO compared to its steady-state ground state spectrum (see Supporting Information for experimental details and measurements in water). The ground state is characterized by two major features corresponding to Fe 2p→3d (e$_g$) (708.7 eV) and Fe 2p→CN$^-$ (2π*) (711.3 eV) excitations.[21] The small intensity at about 705.5 eV is most likely due to minor impurities resulting from the sample preparation. The transient difference spectrum exhibits two depletion features (negative intensities) that result from a reduced absorption of the depopulated electronic ground state. Additionally, a new resonance can be observed at energies below the first depletion as well as a shift of the main edge to higher energies (see positive intensity at about 710 eV). These features are similar to previously observed transient L-edge absorption signatures of [Ru-(bpy)$_3$]$^{2+}$[26] and, on the picosecond timescales probed within this study, can therefore be expected to correspond to the occurrence of the ^{3}MLCT state.[8] This assignment can be further substantiated by studying the relaxation dynamics presented in Figure 1d. The delay traces are acquired at

energies roughly corresponding to the spectral minimum and maximum. The decay of excited-state intensity as well as the ground-state recovery can be modeled with a single-exponential function. The fit yields a lifetime of (17 ± 2) ps, which is in excellent agreement with the previously reported 19 ps lifetime of the ^{3}MLCT state.[8]

As the ^{3}MLCT state of [Fe(bpy)(CN)$_4$]$^{2-}$ in DMSO is the lowest state in energy within the triplet manifold, its electronic structure can be accessed with ground-state theories, such as DFT. This allows the ground and excited-state L-edge absorption to be modelled using the restricted open-shell configuration interaction singles (ROCIS) method[27] (see Supporting Information). DFT/ROCIS employs a slightly parametrized formulation of the configuration interaction problem based on a DFT reference, thus being able to explicitly treat multiplet effects while also implicitly accounting for dynamic electron correlation. The simulated difference spectrum is shown in Figure 2a. It is
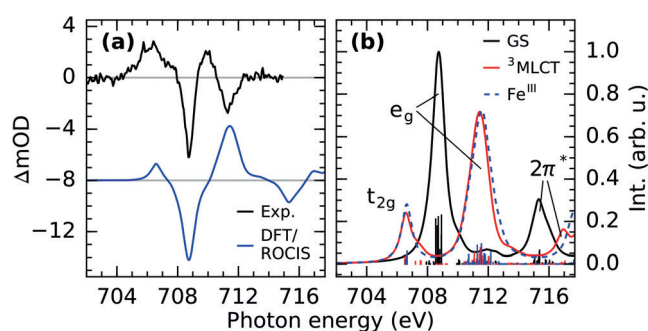

Figure 2. a) Transient L$_3$-edge absorption spectrum of the ^{3}MLCT state of [Fe(bpy)(CN)$_4$]$^{2-}$ and spectrum simulations based on DFT/ROCIS. b) Simulated transitions and convoluted spectra of the ground state (GS), the ^{3}MLCT state as well as the fully oxidized [Fe(bpy)(CN)$_4$]$^{1-}$ (denoted as Fe^{III}).

generated as the difference between the unnormalized ^{3}MLCT and ground-state spectra. The difference is then normalized to the maximum depletion of the experimental spectrum from Figure 1c, which is shown for comparison. The simulation exhibits good agreement with the experiment and reproduces all experimentally detected features. The individual spectra of the ground and ^{3}MLCT state are shown in Figure 2b. For comparison, the spectrum of the fully oxidized [Fe^{III}(bpy)(CN)$_4$]$^{1-}$ is additionally displayed. The ground state spectrum is normalized to its maximum. The ^{3}MLCT and Fe^{III} spectra are scaled accordingly. When analyzing the individual transitions, the additional pre-edge feature at 706.3 eV appearing for the ^{3}MLCT state and the Fe^{III} species can be assigned to be of Fe 2p→t$_{2g}$ character. Within the orbital approximation, the arising pre-edge in the experimental difference spectrum therefore directly probes the depopulation of the formerly fully filled t$_{2g}$ orbitals. The calculation further confirms the experimentally observed shift of the main edge (denoted as e$_g$) to higher energies for the ^{3}MLCT state. The shift is accompanied by a broadening caused by an increase in multiplet features due to the loss of a t$_{2g}$ electron and thus an increase of unpaired 3d spins in the core-excited

state. Again, an almost identical behavior can be observed for the Fe[III] species. The shift of 2.7 eV in both species is however slightly bigger than what is typically observed when comparing Fe[II] and Fe[III] complexes.[17–19,28] We suspect this is due to the incomplete description of the multiplet structure by the DFT/ROCIS method resulting in an overestimation of the energy of the main edge maximum, as has previously been observed for the similar case of $[Fe^{III}(tacn)_2]^{3+}$.[27] Lastly, a reduced Fe 2p→CN$^-$ ($2\pi^*$) excitation can be observed for the ^{3}MLCT state. As a result of the character of the involved orbitals, the excitation has previously been identified as a probe of π-back-donation.[18,21] The decrease of the feature in the ^{3}MLCT state therefore also reflects the reduced t_{2g} occupation and thus provides more evidence for the local Fe[III] character of the ^{3}MLCT state. The calculation, however, consistently overestimates the energy of the excitations (see Supplementary Information). Such difficulties of correctly reproducing the energy of L-edge transitions involving ligand-centered orbitals have also been observed in ab initio restricted active space simulations of Fe[II] and Fe[III] hexacyanides.[28,29]

Having identified the photo-induced local oxidation of the metal center in the ^{3}MLCT state, its quantitative relation to the charge and spin density distributions can be investigated. They are displayed as differences between ^{3}MLCT and

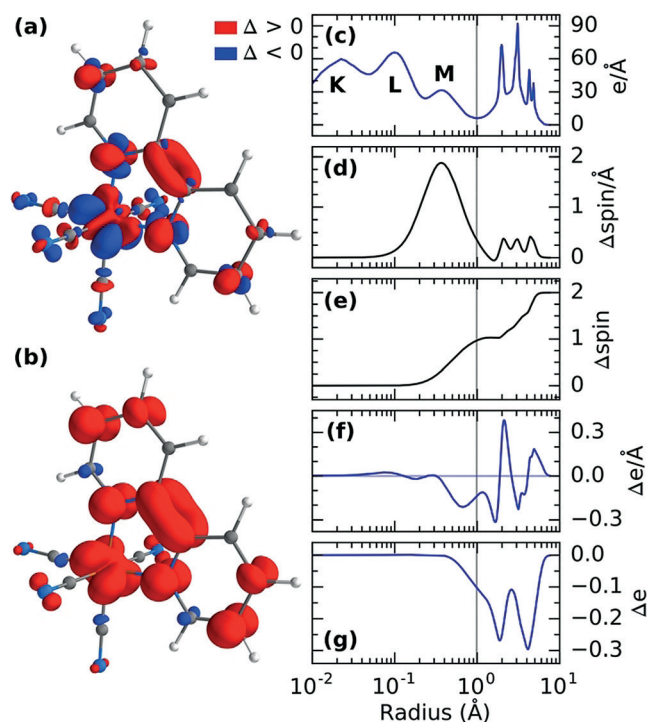***Figure 3.*** a) Charge and b) spin density differences between the ^{3}MLCT and ground state of $[Fe(bpy)(CN)_4]^{2-}$ plotted at an isovalue of 0.005. c) Ground-state charge density of $[Fe(bpy)(CN)_4]^{2-}$ as a function of the radius around the Fe center. d) Spin density difference, as well as e) the integrated spin density difference showing the occurrence of a single spin in the M shell and another single spin distributed over the ligands. f) Charge density difference showing the loss and gain of electronic charge distributed over the whole molecule. g) Integrated charge density difference yielding a loss of 10% of an electronic charge e at the Fe center.

ground state in Figure 3 a,b for the Franck-Condon (FC) region to analyze variations of spin and charge densities independent of structural influences. The validity of this approach can be motivated by the insubstantial structural changes in the ^{3}MLCT state, which are also reflected in the similarity of the calculated spectra for the FC region and the optimized ^{3}MLCT structure (see Supporting Information). Such small structural responses have also been observed for ^{3}MLCT states in other Fe[II][7] as well as Ru[II] photosensitizers.[9,26]

At first sight, the charge and spin density differences in Figure 3 a,b confirm an intuitive perception of a charge-transfer state. As expected from the nominal Fe(t_{2g})→bpy (π*) MLCT excitation character and in agreement with the L-edge XAS measurements, charge density decreases at the metal center in the shape of a t_{2g}-like orbital, while it is increased as delocalized π density on the bpy ligand (compare Figure 3 a). Similarly, spin density appears at the metal center as well as spread out over the ligand corresponding to the two unpaired spins of the ^{3}MLCT state (compare Figure 3 b). However, in particular the charge density difference in Figure 3 a exhibits additional features that require a more detailed analysis of quantitative charge and spin density changes resulting from the optical excitation.

For that purpose, we turn to Figure 3 c, where the ground state charge density is plotted as a radial distribution around the Fe center in analogy to work by Johansson et al.[12] and Kubin et al.[13] The charge density is calculated as the sum of spin-up and spin-down electronic charges e within a radial interval. For small radii below 1 Å, the plot shows the Fe K, L, and M shell, while charge density beyond 1 Å can be assigned to the different ligands. The vertical line at about 1 Å marks half the average distance between the Fe center and its nearest neighbors and can be used to distinguish metal from ligand charge density in agreement with the valley in electron density between the metal M shell and the ligands.

With the ground state charge density in Figure 3 c providing spatial orientation, we turn to the spin density difference between ^{3}MLCT and ground state shown in Figure 3 d. In the closed-shell singlet ground state, no unpaired spins are present and the spin density is zero at all points in space. The spin density difference between the ^{3}MLCT and the ground state is therefore calculated as the difference between spin-up and spin-down electrons of the ^{3}MLCT state. If compared to Figure 3 c, spin density can be identified to appear in the Fe M shell as well as distributed over the ligands. When radially integrated as displayed in Figure 3 e, this amounts to one spin at the metal and another spin at up to around 6 Å. The ^{3}MLCT state therefore creates two spatially separated spins in agreement with the traditional way of charge-transfer state identification[7,8] based on for example, Mulliken spin analysis.[30]

The charge density difference between ^{3}MLCT and ground state is displayed in Figure 3 f. The charge density indeed decreases in the Fe M shell and increases on the ligand at 2.1 Å and 5 Å, as expected for a charge-transfer state. However, significant loss of charge can also be seen at around 1.6 Å and 3.2 Å. When integrated along the radius until 1 Å (compare Figure 3 g), only an effective charge loss of 10% of

a full electronic charge e can be observed at the Fe center. This small change can be rationalized by compensating effects resulting from changes in metal-ligand covalency concomitant to the changes in orbital population. When comparing Fe^II and Fe^III complexes within the same high-field ligand cage, the removal of a metal electron reduces Coulomb repulsion between metal and ligand. This facilitates an increase in σ-donation as has been indicated by different spectroscopies across a wide energy range.[18,31,32] A similar effect can be observed in our case. In Figure 3 a, it can be seen how the loss of π-shaped charge density from the Fe t_{2g} orbital is counter-balanced by an increase in σ-donation from the N atoms of the bpy as well as the to a smaller extend from the C atoms of the CN⁻ ligands. At the N sites of the bpy ligand, this results in a charge decrease with σ character that explains the loss of charge density at 1.6 Å and 3.2 Å (see Figure 3 f).

With an effective loss of only 10 % of a metal electronic charge as a result of the formation of the ³MLCT state, the observed redistribution of electron density compensates for a large fraction of the charge of the transferred Fe 3d electron. This is similar to observations by Johansson et al. for the case of Fe^II and Fe^III haem a.[12] It indicates that the metal center strives to uphold its noble-gas-like configuration in terms of absolute electronic charge density, even if a metal-derived t_{2g} orbital is depopulated. The small loss of metal charge is in contrast to the character nominally associated with MLCT states. Yet it appears to be characteristic for transition-metal dyes employing strong σ-donors, such as N-heterocyclic carbenes, cyanide, and polypyridyl ligands. The separation of electronic charge in ³MLCT states can therefore not be considered a criterion with which feasibility or even efficiency of interfacial charge-injection from transition-metal dyes can be described, as the absence of charge separation in $[Fe(bpy)(CN)_4]^{2-}$ does not inhibit its use for semiconductor sensitization.[14,15] The unpaired spin density residing at the ligand on the other hand provides a suitable picture of electron localization at peripheral parts of the dye necessary for interfacial charge injection. When following intra-molecular and interfacial transfer processes, the spin can therefore be considered the more appropriate quantity for spatially describing the electron.

Similar studies employing time-resolved L-edge XAS at the transition-metal center could be envisioned that shed light on the origin of the poor performance of Fe^II photosensitizers in terms of electron–hole recombination[16] in comparison to Ru^II complexes. Owing to the spatial extent of their 4d shell Ru^II complexes are generally more covalent than their Fe^II counterparts.[33] The compensating effects following an MLCT excitation revealed herein can therefore be expected to be even more efficient, as indicated by previous Ru L-edge measurements.[26] This has possible consequences for the recombination probability of the system. Investigations under in operando conditions[34,35] could aim at following the full oxidation and recombination cycle at a dye–semiconductor interface. With L-edge spectroscopy providing local orbital selectivity, these types of studies will provide a better mechanistic understanding of how charge and spin densities mediate electron transfer in molecular electronic devices.

Conflict of interest

The authors declare no conflict of interest.

[1] B. O'Regan, M. Grätzel, *Nature* **1991**, *353*, 737–740.
[2] W. Gawelda, A. Cannizzo, V. Pham, F. van Mourik, C. Bressler, M. Chergui, *J. Am. Chem. Soc.* **2007**, *129*, 8199–8206.
[3] G. Auböck, M. Chergui, *Nat. Chem.* **2015**, *7*, 629–633.
[4] W. Zhang, et al., *Nature* **2014**, *509*, 345–348.
[5] K. S. Kjær, et al., *Struct. Dyn.* **2017**, *4*, 044030.
[6] Y. Liu, P. Persson, V. Sundström, K. Wärnmark, *Acc. Chem. Res.* **2016**, *49*, 1477–1485.
[7] L. A. Fredin, M. Pápai, E. Rozsályi, G. Vankó, K. Wärnmark, V. Sundström, P. Persson, *J. Phys. Chem. Lett.* **2014**, *5*, 2066–2071.
[8] W. Zhang, et al., *Chem. Sci.* **2017**, *8*, 515–523.
[9] B. E. Van Kuiken, N. Huse, H. Cho, M. L. Strader, M. S. Lynch, R. W. Schoenlein, M. Khalil, *J. Phys. Chem. Lett.* **2012**, *3*, 1695–1700.
[10] D. Moonshiram, P. Garrido-Barros, C. Gimbert-Suriñach, A. Picón, C. Liu, X. Zhang, M. Karnahl, A. Llobet, *Chem. Eur. J.* **2018**, *24*, 6464–6472.
[11] R. M. Jay, et al., *J. Phys. Chem. Lett.* **2018**, *9*, 3538–3543.
[12] M. P. Johansson, M. R. A. Blomberg, D. Sundholm, M. Wikström, *Biochim. Biophys. Acta Bioenerg.* **2002**, *1553*, 183–187.
[13] M. Kubin, et al., *Chem. Sci.* **2018**, *9*, 6813–6829.
[14] M. Yang, D. W. Thompson, G. J. Meyer, *Inorg. Chem.* **2000**, *39*, 3738–3739.
[15] M. Yang, D. W. Thompson, G. J. Meyer, *Inorg. Chem.* **2002**, *41*, 1254–1262.
[16] T. C. B. Harlang, et al., *Nat. Chem.* **2015**, *7*, 883–889.
[17] E. C. Wasinger, F. M. F. de Groot, B. Hedman, K. O. Hodgson, E. I. Solomon, *J. Am. Chem. Soc.* **2003**, *125*, 12894–12906.
[18] R. K. Hocking, E. C. Wasinger, F. M. F. de Groot, K. O. Hodgson, B. Hedman, E. I. Solomon, *J. Am. Chem. Soc.* **2006**, *128*, 10442–10451.
[19] R. K. Hocking, E. C. Wasinger, Y. Yan, F. M. F. DeGroot, F. A. Walker, K. O. Hodgson, B. Hedman, E. I. Solomon, *J. Am. Chem. Soc.* **2007**, *129*, 113–125.
[20] S. P. Cramer, F. M. F. DeGroot, Y. Ma, C. T. Chen, F. Sette, C. A. Kipke, D. M. Eichhorn, M. K. Chan, W. H. Armstrong, *J. Am. Chem. Soc.* **1991**, *113*, 7937–7940.
[21] R. M. Jay, S. Eckert, M. Fondell, P. S. Miedema, J. Norell, A. Pietzsch, W. Quevedo, J. Niskanen, K. Kunnus, A. Föhlisch, *Phys. Chem. Chem. Phys.* **2018**, *20*, 27745–27751.

[22] K. Godehusen, T. Richter, P. Zimmermann, P. Wernet, *J. Phys. Chem. A* **2017**, *121*, 66–72.

[23] N. Huse, T. K. Kim, L. Jamula, J. K. McCusker, F. M. F. de Groot, R. W. Schoenlein, *J. Am. Chem. Soc.* **2010**, *132*, 6809–6816.

[24] H. E. Toma, M. S. Takasugi, *J. Solution Chem.* **1983**, *12*, 547–561.

[25] K. S. Kjær, et al., *Phys. Chem. Chem. Phys.* **2018**, *20*, 4238–4249.

[26] W. Gawelda, M. Johnson, F. M. F. de Groot, R. Abela, C. Bressler, M. Chergui, *J. Am. Chem. Soc.* **2006**, *128*, 5001–5009.

[27] M. Roemelt, D. Maganas, S. DeBeer, F. Neese, *J. Chem. Phys.* **2013**, *138*, 204101.

[28] K. Kunnus, et al., *J. Phys. Chem. B* **2016**, *120*, 7182–7194.

[29] R. V. Pinjari, M. G. Delcey, M. Guo, M. Odelius, M. Lundberg, *J. Chem. Phys.* **2014**, *141*, 124116.

[30] R. S. Mulliken, *J. Chem. Phys.* **1955**, *23*, 1833–1840.

[31] L. H. Jones, *Inorg. Chem.* **1963**, *2*, 777–780.

[32] C. J. Pollock, M. U. Delgado-Jaime, M. Atanasov, F. Neese, S. DeBeer, *J. Am. Chem. Soc.* **2014**, *136*, 9453–9463.

[33] J. K. McCusker, *Science* **2019**, *363*, 484–488.

[34] K. R. Siefermann, et al., *J. Phys. Chem. Lett.* **2014**, *5*, 2753–2759.

[35] E. Baldini, T. Palmieri, T. Rossi, M. Oppermann, E. Pomarico, G. Auböck, M. Chergui, *J. Am. Chem. Soc.* **2017**, *139*, 11584–11589.